NASA TECHNICAL NOTE

NASA TN D-3280

NASA TN D-3280

ANALYTICAL INVESTIGATION OF THE MOTION OF A CLAMSHELL-TYPE HEAT SHIELD ON DEPLOYMENT FROM A PARENT VEHICLE IN THE ATMOSPHERE

by Ross L. Goble

Langley Research Center
Langley Station, Hampton, Va.

NATIONAL AERONAUTICS AND SPACE ADMINISTRATION • WASHINGTON, D. C. • MARCH 1966

NASA TN D-3280

ANALYTICAL INVESTIGATION OF THE MOTION OF A CLAMSHELL-TYPE HEAT SHIELD ON DEPLOYMENT FROM A PARENT VEHICLE IN THE ATMOSPHERE

By Ross L. Goble

Langley Research Center
Langley Station, Hampton, Va.

NATIONAL AERONAUTICS AND SPACE ADMINISTRATION

For sale by the Clearinghouse for Federal Scientific and Technical Information
Springfield, Virginia 22151 – Price $2.00

ANALYTICAL INVESTIGATION OF THE MOTION OF A CLAMSHELL-TYPE HEAT SHIELD ON DEPLOYMENT FROM A PARENT VEHICLE IN THE ATMOSPHERE

By Ross L. Goble
Langley Research Center

SUMMARY

The equations of motion for the deployment of the clamshell-type heat shield are developed herein for the various phases of separation from an accelerating vehicle in the sensible atmosphere. The shield motion is planar and is divided into four phases: Phase 1, translation from the closed position to pivot contact; phase 2, rotation about pivot; phase 3, translation on and rotation about pivot to release; and phase 4, translation and rotation away from the parent vehicle. Closed-form solution of the linear equation of motion in phase 1 for constant lift and drag permits description of the translation velocity. An iterative numerical integration technique is used to solve the nonlinear equations of angular motion for phases 2, 3, and 4. The release equation is also established. Specific applications of the analysis to deployment of the Nimbus heat-shield configurations, used on many NASA projects, under various vehicular acceleration and aerodynamic loading conditions are included.

INTRODUCTION

Heat shielding is required for the protection of many types of flight payloads which have telemetry equipment, delicate instrumentation, and other reentry and space experiment apparatus. One specific requirement in the Project Fire experiment (ref. 1), for example, was the shielding of the quartz windows in the forward section of the payload from atmospheric abrasion during the early flight stages. In some experiments, the shield is an integral component of the payload. Often, however, the nature of the experiment requires deployment of the heat shield during flight to permit proper functioning of the protected apparatus. Motion analysis of the shield intended for such use is required so that optimum design parameters and ejection conditions may be selected to ensure the desired deployment. The analysis herein is based on the spring method of shield deployment such as has been successfully used on the Nimbus shroud configuration, which includes the basic configuration used or intended for use on such projects as Fire, Echo II, Gemini Docking, Earth Orbiting Geophysical Observatory (EOGO), Nimbus, and other space experiments. Analysis also permits description of the shield trajectory after release. This

description is important in determining the most desirable release conditions which will not only preclude shield mechanical interference with any portion of the vehicle after release, but will also satisfy a predetermined minimum safe clearance requirement.

The studies presented herein may be effectively utilized in the establishing of optimum ejection criteria for future projects using the spring-ejected shroud. It is readily seen that many of the problems pertinent to the motion of the clamshell-type shield herein described will pertain to any clamshell-shield separation regardless of the deployment means.

It is convenient to consider the shield planar motion in four phases: phase 1, translation from the closed position to pivot contact; phase 2, rotation about pivot; phase 3, translation on and rotation about pivot to release; and phase 4, translation and rotation away from the parent vehicle. There are four parallel springs used in the Nimbus shield-ejection scheme, two acting at the aft end of the shield and two acting in the conical section near the nose. The springs act through phase 1 in translating the shield from the closed position to pivot contact. The two aft springs then serve the purpose of holding the shield pivot fitting against the booster pivot until shield release is effected at the end of phase 3. Also, the forward springs provide the force necessary to initiate and sustain rotation through phases 2 and 3. The springs in this ejection scheme are designed to act until expanded to free length.

Separation dynamics for vacuum flight have been studied for the two-body system in references 2 and 3 and for heat shields in references 4 and 5. The consideration of aerodynamic effects has been generally confined to airplane escape capsules (ref. 6) and to atmospheric abort of space capsules from boosters (ref. 7). The presented method is similar to that described in references 4 and 5 but with the inclusion of aerodynamics.

The purpose of this study is to investigate some of the factors which affect deployment and to ascertain their significance. The dynamic pressure, which has been generally neglected in related published literature, is one of the most important factors influencing shield deployment. Other factors treated in the application of the analytical method to physical systems are vehicular longitudinal acceleration, spring force, and change in length of the cylindrical portion of the shield.

SYMBOLS

Measurements for this investigation were taken in the U.S. Customary System of Units. Equivalent values are indicated herein in the International System (SI) in the interest of promoting use of this system in future NASA reports. Details concerning the use of SI, together with physical constants and conversion factors, are given in reference 8.

A forward spring initial preload, in. (m)

a_l net vehicular longitudinal acceleration, g units

B	aft spring initial preload, in. (m)
C_1, C_2, C_3	constants of integration
c	radial distance to shield center of gravity from pivot point, in. (m)
D	aerodynamic drag force, lbf (N)
d	total shield diameter (fig. 1), in. (m)
E_k	kinetic energy, in-lbf (J)
e	displacement of pivot along release plane, in. (m)
e_r	displacement of pivot at time of release, in. (m)
F_a	forward spring force (eq. (26)), lbf (N)
F_b	aft spring force (eq. (26)), lbf (N)
F_{fb}	kinetic friction force at shield base, lbf (N)
F_{fp}	static friction force at pivot, lbf (N)
g	acceleration equivalent to earth gravity, 386 in/sec^2 (9.8 m/sec^2)
H	pivot reaction in x-direction (fig. 2(b)), lbf (N)
h	distance from shield center of gravity to shield outside edge (fig. 1), in. (m)
i,j	integers
I_{cg}	half-shield mass moment of inertia about its center of gravity, lb-sec^2-in. (N-sec^2-m)
I_O	half-shield mass moment of inertia about the pivot center of rotation, lb-sec^2-in. (N-sec^2-m)
K_1	constant for phase 1 motion (eq. (8)), in/sec^2 (m/sec^2)
k	superscript indicating kth iteration for numerical method, dimensionless
k_a	forward spring constant, lb/in. (N/m)
k_b	aft spring constant, lb/in. (N/m)
L	aerodynamic lift force, lbf (N)
$\bar{L}$	Lagrangian, $E_k - U_p$, in-lbf (J)

M	aerodynamic moment, in-lbf (N-m)
m	mass of shield half, lbm-sec^2/in. (kg)
$n,n+1$	successive steps in the numerical solution, unitless
p	distance from pivot center of rotation to contact point of aft spring, in. (m)
q	dynamic pressure, lbf/ft^2 (N/m^2)
q_i	generalized coordinate having dimensions of coordinate used
q_j	constant used in clearance equations (48) and (49)
r	distance from pivot center of rotation to contact point of forward spring, in. (m)
r_j	distance from shield-half center of gravity to clearance point considered (fig. 3), in. (m)
t	time variable, sec
t_1,t_2,t_3	time intervals for deployment (fig. 9), sec
U_p	potential energy, in-lbf (J)
V	pivot reaction in y-direction (fig. 2(b)), lbf (N)
W	work done by a force, in-lbf (J)
W_D	work due to aerodynamic drag, in-lbf (J)
W_L	work due to aerodynamic lift, in-lbf (J)
W_M	work due to aerodynamic moment, in-lbf (J)
$W_{F,fb}$	work due to friction force, in-lbf (J)
x	longitudinal coordinate of shield center of gravity from reference axis (fig. 1), in. (m)
x_j	longitudinal coordinate of clearance point from reference axis (eq. (49)), in. (m)
x_p	pivot point longitudinal displacement used in virtual work (eq. (26)), in. (m)
x^*	location of shield center of gravity measured from shield base (fig. 1), in. (m)

y lateral coordinate of shield center of gravity from reference axis (fig. 1), in. (m)

y^* location of shield center of gravity measured from shield parting plane edge (fig. 1), in. (m)

$y_A = y - y_a$, in. (m)

$y_a = r\left[\cos\theta_{ro} - \cos(\theta + \theta_{ro})\right]$, in. (m)

$y_B = y - y_b$, in. (m)

$y_b = p\left[\cos\theta_{po} - \cos(\theta + \theta_{po})\right]$, in. (m)

y_c shield center of gravity lateral displacement at pivot contact, in. (m)

$y_e = y_c - y^*$

y_j lateral coordinate of clearance point from reference axis (eq. (48)), in. (m)

y_p pivot point lateral displacement used in virtual work (eq. (26)), in. (m)

$y_r = y - y^*$

Δ time interval prefix used in numerical solution

δ prefix used with linear variables to indicate virtual displacement or virtual work

$\epsilon, \epsilon_1, \epsilon_2$ error terms used in numerical solution

θ angle of rotation, shield base from original position, radian

θ_o initial value of θ for a given phase, radian

θ_{co} reference angle between shield base and center-of-gravity location, radian (See fig. 2(a).)

θ_{po} reference angle between shield base and aft spring point of contact, radian (See fig. 2(a).)

θ_{ro} reference angle between shield base and forward spring point of contact, radian (See fig. 2(a).)

μ coefficient of static friction

μ_s coefficient of sliding friction

ξ orientation of pivot relative to shield outer surface (fig. 2(b)), radian

ϕ_j reference angle for jth clearance point (fig. 3), radian

$\psi = \theta - \xi$, radian, (fig. 2(b))

Dots over variables indicate differentiation with respect to time.

DERIVATION OF EQUATIONS OF MOTION

The derivation of the equations of motion for the rigid body is developed in this section for the four basic phases of operation. Also derived is the equation defining the conditions governing full release of the shield from the parent vehicle. Lagrange's equation is utilized in developing the equations of motion for all phases.

Assumptions Pertinent to the Analysis

The considerations which have been employed in the derivation in providing an adequate mathematical model to the physical system under investigation are as follows:

(1) The vehicle is the inertial reference for the heat shield motion.

(2) At the inception of motion the starting friction force is neglected.

(3) The coefficient of kinetic friction is assumed to be independent of the translational velocity on the pivot.

(4) The Coriolis effect during translation off the pivot is neglected.

(5) The change in the center of rotation during translation off the pivot is considered to be sufficiently small as to be negligible.

(6) The spin rate of the parent vehicle is assumed to be negligible in the analysis. It is also assumed that no roll motion of the shroud halves occurs during deployment.

(7) The heat shield is assumed to be a rigid body.

(8) The two halves of the clamshell shield act independently.

(9) The aerodynamics including flow-field interference effects of the heat shield half are known. Induced aerodynamic loading due to deployment velocities $\dot{\theta}$, $\dot{y}$, and $\dot{x}$ have not been considered in the derivation.

Phase 1 - Translation to Pivot Contact

If the coordinate system in figure 1 is used, the potential energy of the system is:

$$U_p = \frac{1}{2} k_a(A - y_r)^2 + \frac{1}{2} k_b(B - y_r)^2 \tag{1}$$

where $y_r = y - y^*$, the displacement of the shield parting plane edge, and A and B are the preload deflections of the forward and aft springs, respectively.

The kinetic energy is

$$E_k = \frac{1}{2} m\dot{y}^2 \tag{2}$$

The Lagrangian $\bar{L}$ is given by $E_k - U_p$, and Lagrange's equation for the system is

$$\frac{d}{dt}\frac{\partial \bar{L}}{\partial \dot{y}} - \frac{\partial \bar{L}}{\partial y} = \frac{\partial W}{\partial y} \tag{3}$$

The forces (fig. 1) acting on the shield are the friction force F_{fb}, lift, drag, aerodynamic pitching moment, and the longitudinal acceleration force $a_l m$. The virtual work can be described as

$$\delta W = \delta W_{F,fb} + \delta W_L \tag{4}$$

Since

$$F_{fb} = \mu_s\left(D + a_l m\right)$$

then

$$\delta W_{F,fb} = -\mu_s\left(D + a_l m\right)\delta y \tag{5}$$

also

$$\delta W_L = L\,\delta_y \tag{6}$$

The aerodynamic moment and the forces in the x-direction do no work since the plane motion is confined to pure translation in the y-direction by

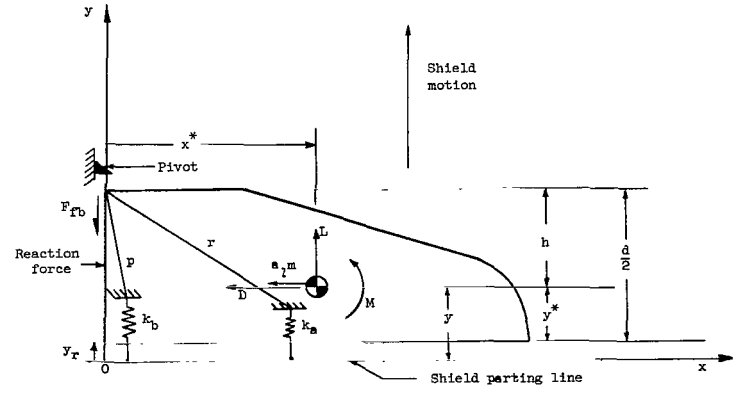

Figure 1.- Heat-shield model. Phase 1, translation.

constraints which preclude rotation and x-translation in this phase. Using the general relation for virtual work

$$\delta W = \sum_{i=1}^{\infty} \frac{\partial W}{\partial q_i} \delta q_i$$

and expanding in terms of the single generalized coordinate y yields

$$\delta W = \frac{\partial W}{\partial y} \delta y$$

or, after substitution of equations (5) and (6) for δW,

$$-\mu_s (D + a_l m)\delta y + L\, \delta y = \frac{\partial W}{\partial y} \delta y$$

Simplifying and equating coefficients, therefore, yields

$$\frac{\partial W}{\partial y} = L - \mu_s (D + a_l m)$$

Operating on equation (3) with substitution of the Lagrangian and $\partial W/\partial y$ yields

$$m\ddot{y} - k_a (A - y + y^*) - k_b (B - y + y^*) = L - \mu_s (D + a_l m) \tag{7}$$

Rearranging yields the differential equation

$$\ddot{y} + \left(\frac{k_a + k_b}{m}\right) y = \frac{1}{m}\left[k_a (A + y^*) + k_b (B + y^*) + L - \mu_s (D + a_l m)\right] \tag{8}$$

Since motion in this phase is nearly impulsive, it is assumed that aerodynamic interference effects between the opening clamshell halves can be neglected. Thus, the aerodynamic forces in the absence of changing angle of attack may be considered to be constant for this phase. The right-hand side of equation (8) is therefore a constant which may be called K_1. The complete solution of the nonhomogeneous equation (8) is thus:

$$y = C_1 \cos\sqrt{\frac{k_a + k_b}{m}}\, t + C_2 \sin\sqrt{\frac{k_a + k_b}{m}}\, t + C_3 \tag{9}$$

Substituting the particular integral $y = C_3$ into equation (8), with the right-hand side of equation (8) being replaced by K_1, and differentiating yields

$$C_3 = \frac{K_1 m}{k_a + k_b}$$

Substitution of the appropriate initial conditions, $t = 0$, $y = y^*$, into solution (9) yields

$$C_1 = - \frac{K_1 m}{k_a + k_b} + y^*$$

Differentiating equation (9) with respect to time and substituting the initial conditions $t = 0$, $\dot{y} = 0$ yields $C_2 = 0$; therefore, the complete solution with arbitrary constants evaluated and some rearrangements made is

$$y = \left(y^* - \frac{K_1 m}{k_a + k_b} \right) \cos \sqrt{\frac{k_a + k_b}{m}}\, t + \frac{K_1 m}{k_a + k_b} \tag{10}$$

from which the solution for time t is

$$t = \sqrt{\frac{m}{k_a + k_b}} \cos^{-1} \left(\frac{y - \dfrac{K_1 m}{k_a + k_b}}{y^* - \dfrac{K_1 m}{k_a + k_b}} \right) \tag{11}$$

The translation velocity relation obtained by differentiating equation (10) is

$$\dot{y} = - \left(y^* - \frac{K_1 m}{k_a + k_b} \right) \sqrt{\frac{k_a + k_b}{m}} \sin \sqrt{\frac{k_a + k_b}{m}}\, t$$

or by substituting for t from equation (11) and simplifying is

$$\dot{y} = \left(\frac{K_1 m}{k_a + k_b} - y^* \right) \sqrt{\frac{k_a + k_b}{m} \left[1 - \left(\frac{y - \dfrac{K_1 m}{k_a + k_b}}{y^* - \dfrac{K_1 m}{k_a + k_b}} \right)^2 \right]} \tag{12}$$

Knowledge of the center-of-gravity displacement (for example, $y = y_c$) at which pivot contact occurs permits solution of equation (12). When $\dot{y}_c$ is determined, the initial value of the angular velocity for phase 2 can be established in the following manner.

Phase 2 - Rotation About Pivot

If it is assumed that no energy is lost in impact, all translational energy is converted to rotational energy about the pivot at the instant of pivot contact, or

$$\frac{1}{2} m\dot{y}_c^2 = \frac{1}{2} I_0 \dot{\theta}_o^2 \tag{13}$$

Making substitutions for $\dot{y}_c$ and simplifying yields

$$\dot{\theta}_o = \left(\frac{K_1 m}{k_a + k_b} - y^*\right)\sqrt{\frac{k_a + k_b}{I_0}\left[1 - \left(\frac{y_c - \frac{K_1 m}{k_a + k_b}}{y^* - \frac{K_1 m}{k_a + k_b}}\right)^2\right]} \tag{14}$$

The top and bottom springs have displaced an amount $y_e = y_c - y^*$ at the instant of pivot contact. Thus, the potential energy of the system taking the datum as shown in figure 2 is

$$U_p = a_1 mc \sin(\theta + \theta_{co}) + \frac{1}{2} k_a (A - y_a - y_e)^2 + \frac{1}{2} k_b (B - y_b - y_e)^2 \tag{15}$$

where

$$\left.\begin{aligned} y_a &= r\left[\cos\theta_{ro} - \cos(\theta + \theta_{ro})\right] \\ y_b &= p\left[\cos\theta_{po} - \cos(\theta + \theta_{po})\right] \end{aligned}\right\} \tag{16}$$

and equation (15) is valid for $y_a + y_e \leqq A$ and $y_b + y_e \leqq B$. The kinetic energy of the system is

$$E_k = \frac{1}{2} I_0 \dot{\theta}^2 \tag{17}$$

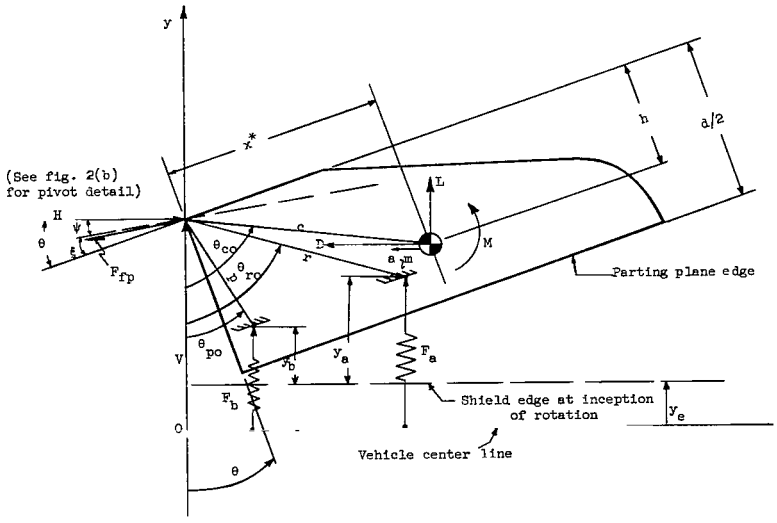

(a) Geometry and release plane description.

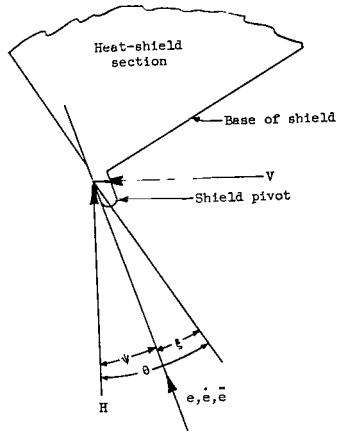

(b) Detail of pivot point and release plane.

Figure 2.- Heat-shield model. Phase 2, rotation.

If the substitution for y_a and y_b is made in equation (15), the Lagrangian then becomes

$$\bar{L} = \frac{1}{2} I_0 \dot{\theta}^2 - a_l mc \sin(\theta + \theta_{co}) - \frac{1}{2} k_a \left\{ A - r\left[\cos \theta_{ro} - \cos(\theta + \theta_{ro})\right] - y_e \right\}^2$$

$$- \frac{1}{2} k_b \left\{ B - p\left[\cos \theta_{po} - \cos(\theta + \theta_{po})\right] - y_e \right\}^2 \qquad (18)$$

Operating on $\bar{L}$ with respect to the generalized coordinate θ by Lagrange's equation

$$\frac{d}{dt}\left(\frac{\partial \bar{L}}{\partial \dot{\theta}}\right) - \frac{\partial \bar{L}}{\partial \theta} = \frac{\partial W}{\partial \theta}$$

yields

$$I_0 \ddot{\theta} + a_l mc \cos(\theta + \theta_{co}) - k_a \left\{ A - r\left[\cos \theta_{ro} - \cos(\theta + \theta_{ro})\right] - y_e \right\} r \sin(\theta + \theta_{ro})$$

$$- k_b \left\{ B - p\left[\cos \theta_{po} - \cos(\theta + \theta_{po})\right] - y_e \right\} p \sin(\theta + \theta_{po}) = \frac{\partial W}{\partial \theta} \qquad (19)$$

For a virtual angular displacement $\delta\theta$ the virtual work contributions of the aerodynamic forces (where L, D, and M are with respect to the shield center of gravity) are

$$\delta W_L = Lc\left[\cos\left(\theta + \theta_{co}\right) - \cos\left(\theta + \theta_{co} + \delta\theta\right)\right] \tag{20a}$$

$$\delta W_D = -Dc\left[\sin\left(\theta + \theta_{co} + \delta\theta\right) - \sin\ \theta + \theta_{co}\right)\right] \tag{20b}$$

and

$$\delta W_M = M\ \delta\theta$$

Expanding the double angles and making the small angle approximations $\cos\ \delta\theta = 1$, $\sin\ \delta\theta = \delta\theta$ yields, after simplification,

$$\delta W_L = Lc\ \sin\left(\theta + \theta_{co}\right)\delta\theta \tag{21a}$$

$$\delta W_D = -Dc\ \cos\left(\theta + \theta_{co}\right)\delta\theta \tag{21b}$$

and also

$$\delta W_M = M\ \delta\theta \tag{22}$$

Again, employing the relation

$$\delta W = \sum_{i=1}^{\infty} \frac{\partial W}{\partial q_i}\ \delta q_i$$

and substituting for the virtual work terms with respect to the generalized coordinate θ yields

$$\left[Lc\ \sin\left(\theta + \theta_{co}\right) - Dc\ \cos\left(\theta + \theta_{co}\right) + M\right]\delta\theta = \frac{\partial W}{\partial\theta}\ \delta\theta$$

Equating coefficients and making substitution for $\partial W/\partial\theta$ into equation (19) yields, for the moment relative to the pivot point,

$$I_O\ddot{\theta} + a_l mc \cos(\theta + \theta_{co}) - k_a\left\{A - r\left[\cos\theta_{ro} - \cos(\theta + \theta_{ro})\right] - y_e\right\} r \sin(\theta + \theta_{ro})$$

$$- k_b\left\{B - p\left[\cos\theta_{po} - \cos(\theta + \theta_{po})\right] - y_e\right\} p \sin(\theta + \theta_{po}) = Lc \sin(\theta + \theta_{co})$$

$$- Dc \cos(\theta + \theta_{co}) + M \tag{23}$$

where lift, drag, and pitching moment vary with angle of attack θ and include interference effects. Also, induced aerodynamic loading due to $\dot{\theta}$, $\dot{y}$, and $\dot{x}$ has been assumed to be trivial. Solution of equation (23) for $\ddot{\theta}$ yields

$$\ddot{\theta} = \frac{1}{I_O}\left[\left(k_a\left\{A - r\left[\cos\theta_{ro} - \cos(\theta + \theta_{ro})\right] - y_e\right\} r \sin(\theta + \theta_{ro})\right.\right.$$

$$+ k_b\left\{B - p\left[\cos\theta_{po} - \cos(\theta + \theta_{po})\right] - y_e\right\} p \sin(\theta + \theta_{po})$$

$$\left.\left. - (D + a_l m)c \cos\theta_{co} + Lc \sin(\theta + \theta_{co}) + M\right)\right] \tag{24}$$

which is valid for

$$\left\{A - r\left[\cos\theta_{ro} - \cos(\theta + \theta_{ro})\right] - y_e\right\} \leqq 0$$

$$\left\{B - p\left[\cos\theta_{po} - \cos(\theta + \theta_{po})\right] - y_e\right\} \leqq 0$$

Phase 2 initial conditions are as follows: At $t = t_o$, $\theta = 0$, $\dot{\theta} = \dot{\theta}_o$, $L = L_o$, $D = D_o$, $M = M_o$, and the initial acceleration from equation (24) becomes

$$\ddot{\theta}_o = \frac{1}{I_O}\left[-(D_o + a_l m)c \cos\theta_{co} + k_a(A - y_e) r \sin\theta_{ro}\right.$$

$$\left. + L_o c \sin\theta_{co} + M_o + k_b(B - y_e) p \sin\theta_{po}\right] \tag{25}$$

Solution of the angular displacement θ and its time derivatives may be accomplished by stepwise numerical integration of equation (24) as shown in appendix A.

Developed in the next section are the relations required to analyze translational motion on the pivot.

Phase 3 - Release Action Equations

The externally applied loads (fig. 2) are L, M, D, and $a_l m$; the reactions are H and V; and the spring forces are F_a and F_b. The virtual work of the system is then

$$\delta W = -\left(D + a_l m\right)\delta x + L\,\delta y + M\,\delta\theta + H\,\delta x_p + V\,\delta y_p + F_a\,\delta y_A + F_b\,\delta y_B \qquad (26)$$

where δx_p and δy_p are the respective x and y virtual displacements of the pivot point, and δy_A and δy_B are the y virtual displacements of the forward and aft springs.

The system kinetic energy related to the center of gravity of the shield half is

$$E_k = \frac{1}{2} m\left(\dot{y}^2 + \dot{x}^2\right) + \frac{1}{2} I_{cg}\dot{\theta}^2 \qquad (27)$$

Since the system is originally restrained at the pivot, the following geometric relations in terms of the generalized coordinates x, y, and θ may be written

$$y = x^* \sin\theta + h(1 - \cos\theta) + y_c \qquad (28)$$

$$\left.\begin{aligned} y_p &= y + h\cos\theta - x^*\sin\theta \\ y_A &= y + c\cos\left(\theta + \theta_{co}\right) - r\cos\left(\theta + \theta_{ro}\right) \\ y_B &= y + c\cos\left(\theta + \theta_{co}\right) - p\cos\left(\theta + \theta_{po}\right) \end{aligned}\right\} \qquad (29)$$

$$x = x^*\cos\theta + h\sin\theta \qquad (30)$$

$$x_p = x - h\sin\theta - x^*\cos\theta \qquad (31)$$

Note that relations for y_p and x_p vanish identically but are in a form necessary for establishing the virtual displacement of points actually constrained against possible motion. This useful artifice is commonly employed in virtual work relations in order to permit definition of reactive forces at a point. The time derivatives of equations (28) and (30) are:

$$\dot{y} = \dot{\theta}(x^* \cos\theta + h \sin\theta) \tag{32}$$

$$\ddot{y} = \ddot{\theta}(x^* \cos\theta + h \sin\theta) + \dot{\theta}^2(h \cos\theta - x^* \sin\theta) \tag{33}$$

$$\dot{x} = \dot{\theta}(h \cos\theta - x^* \sin\theta) \tag{34}$$

and

$$\ddot{x} = \ddot{\theta}(h \cos\theta - x^* \sin\theta) - \dot{\theta}^2(x^* \cos\theta + h \sin\theta) \tag{35}$$

Making substitutions into Lagrange's equation and differentiating yields

$$m\ddot{y} = L + V + F_a + F_b \tag{36}$$

$$m\ddot{x} = -(D + a_\gamma m) + H \tag{37}$$

and $\ddot{\theta}$ is redefined in terms of the V- and H-components by

$$I_{cg}\ddot{\theta} = M + H(x^* \sin\theta - h \cos\theta) - V(h \sin\theta + x^* \cos\theta) + F_a\left[r \sin(\theta + \theta_{ro}) - c \sin(\theta + \theta_{co})\right] + F_b\left[p \sin(\theta + \theta_{po}) - c \sin(\theta + \theta_{co})\right] \tag{38}$$

If $\ddot{y}$ and $\ddot{x}$ from equations (33) and (35) are substituted into equations (36) and (37) and the terms rearranged, the pivot reactions, with F_a and F_b expressed in terms of the respective spring preloads and displacements, are

$$V = m\left[\ddot{\theta}(x^* \cos\theta + h \sin\theta) + \dot{\theta}^2(h \cos\theta - x^* \sin\theta)\right] - L - k_a\left\{A - y_e - r\left[\cos\theta_{ro} - \cos(\theta + \theta_{ro})\right]\right\} - k_b\left\{B - y_e - p\left[\cos\theta_{po} - \cos(\theta + \theta_{po})\right]\right\} \tag{39}$$

and

$$H = m\left[\ddot{\theta}(h \cos\theta - x^* \sin\theta) - \dot{\theta}^2(x^* \cos\theta + h \sin\theta)\right] + D + a_\gamma m \tag{40}$$

The instantaneous orientation of the release plane is shown to be at some inclination angle ψ relative to the pivot reaction components. (See fig. 2.) The release plane will be partially determined by the physical configuration of the system. At release, the static equilibrium equation to be satisfied along this plane is

$$V \sin \psi - F_{fp} + H \cos \psi = 0 \tag{41}$$

where the static friction force is defined as

$$F_{fp} = \mu(V \cos \psi - H \sin \psi)$$

Positive H and V have been chosen, as shown in figure 2(b). The equilibrium condition is, after substitution for F_{fp} in equation (41) and simplifying,

$$V(\sin \psi - \mu \cos \psi) + H(\cos \psi + \mu \sin \psi) = 0 \tag{42}$$

After substitutions for V and H from equations (39) and (40) are made, the release relation (42) becomes

$$\left[\left(m\left[\ddot{\theta}(x^* \cos \theta + h \sin \theta) + \dot{\theta}^2(h \cos \theta - x^* \sin \theta)\right] - L - k_a\left\{A - y_e - r\left[\cos \theta_{ro} - \cos(\theta + \theta_{ro})\right]\right\} - k_b\left\{B - y_e - p\left[\cos \theta_{po} - \cos(\theta + \theta_{po})\right]\right\}\right)\right](\sin \psi - \mu \cos \psi)$$

$$+ \left\{m\left[\ddot{\theta}(h \cos \theta - x^* \sin \theta) - \dot{\theta}^2(x^* \cos \theta + h \sin \theta)\right] + D + a_l m\right\}(\cos \psi + \mu \sin \psi) = 0 \tag{43}$$

Equation (43) can thus be evaluated for any θ and is the condition which establishes impending translational motion on the pivot. It can be shown that with slight modification, equation (43) becomes the condition of dynamic equilibrium on the pivot for the translational phase. This modification involves replacing the right-hand side of equation (43) with $-m\ddot{e}$ and μ with μ_s. Since the magnitude of the Coriolis effect due to the shield's rotating about while translating along the pivot is very small relative to other forces in the physical system, the slight retarding effect to the angular motion has been neglected. Also, for the small pivot translational displacement involved, the resultant change in the center of rotation can be neglected, and thus the geometric relations previously established as adequately describing the system are preserved. Therefore, the equation of translational motion (eq. (43) as modified) is, after rearranging,

$$\ddot{e} = \left[\left(\frac{k_a}{m}\left\{A - y_e - r\left[\cos\theta_{ro} - \cos\left(\theta + \theta_{ro}\right)\right]\right\} + \frac{k_b}{m}\left\{B - y_e - p\left[\cos\theta_{po} - \cos\left(\theta + \theta_{po}\right)\right]\right\} - \left[\ddot{\theta}\left(x^*\cos\theta + h\sin\theta\right) + \dot{\theta}^2\left(h\cos\theta - x^*\sin\theta\right)\right] + \frac{L}{m}\right)\right]\left(\sin\psi - \mu_s\cos\psi\right) - \left\{\left[\ddot{\theta}\left(h\cos\theta - x^*\sin\theta\right) - \dot{\theta}^2\left(x^*\cos\theta + h\sin\theta\right) + D + a_l m\right]\right\}\left(\cos\psi + \mu_s\sin\psi\right) \tag{44}$$

Solution of the translational displacement e and its time derivatives is accomplished by the numerical integration technique indicated in appendix B. When the shroud has translated on the pivot a distance e_r, release is effected and the fourth phase of motion begins.

Phase 4 - Free Trajectory Subsequent to Release

At release, the pivot reactions vanish, and the shield begins to translate and rotate away from the vehicle. The initial translational displacements and velocities for this phase are solved by equations (28), (30), (32), and (34), respectively, evaluated at θ equal to the release angle as determined at $e = e_r$. Initial conditions for θ_o and $\dot{\theta}_o$ are also those values established at release. The describing equations of motion, equations (36) to (38), become

$$m\ddot{y} = L \tag{45}$$

$$m\ddot{x} = -\left(D + a_l m\right) \tag{46}$$

and

$$I_{cg}\ddot{\theta} = M \tag{47}$$

Initial conditions for the accelerations are now readily obtained by substitution of the proper values of the aerodynamic effects L, M, and D as determined at θ equal to the release angle. Solution of θ and the corresponding y- and x-coordinates is accomplished numerically as outlined in appendix C.

During the phase 4 motion as described, knowledge of the minimum clearance of the shroud halves from the booster vehicle is important, since any contact could cause damage to the booster and result in possible mission failure. By utilizing the geometry of the shroud, the minimum clearance envelope can be

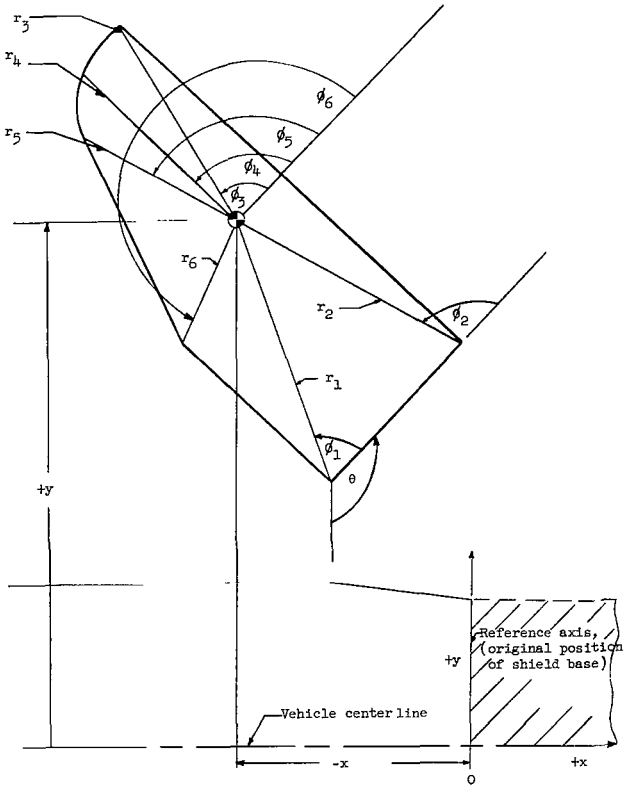

Figure 3.- Clearance point identification.

described by relating coordinates of various points on the shroud to the coordinates of the shroud center of gravity as determined by solution of the displacements from equations (45) and (46). (See appendix C.) Figure 3 indicates the six shroud locations chosen to describe the clearance envelope. The geometric relations utilized are the following:

$$y_j = y + q_j r_j \cos\left(\theta + \phi_j\right) \qquad (48)$$

$$x_j = x - q_j r_j \sin\left(\theta + \phi_j\right) \qquad (49)$$

where

$$j = 1, 2, \ldots, 6$$

$$q_j = 1 \qquad (j = 1 \text{ and } 2)$$

$$q_j = -1 \qquad (j = 3, 4, 5, \text{ and } 6)$$

The absolute displacement of the shroud minimum point can readily be determined by relation (48) at the end of each time interval. Relation (49) can now be solved for the corresponding longitudinal displacement. The lateral clearance is then determined by differencing this near point y_j-displacement with the booster outer radius at the x-coordinate.

GENERAL DISCUSSION AND RESULTS

The equations of motion for a clamshell spring-actuated heat shield, deployed under conditions of aerodynamic and constant vehicular longitudinal acceleration loading, have been derived and presented in the foregoing sections.

In the following sections are presented various factors involved in the application of the analytical equations to the Nimbus long and short heat-shield configurations. Results of a parametric study to determime separation behavior with variations in dynamic pressure, vehicular acceleration, spring force, and shield length are provided.

Simplified Shield Geometry

Mechanical considerations.- The clamshell-type heat shield as used on Project Fire is of the type for which the foregoing analysis is applicable. Several comments pertinent to the actual shield configuration which verify certain aspects of the analytical approach are as follows: First, during the phase 1 motion, the constraint which precludes rotation is provided by a nose latch mechanism. Although this constraint in reality permits a slight negative rotation during this phase, the translational distance at the shield base is so small that the assumption of translation only is valid. Secondly, the spring actuator system is such that for symmetrical shield halves, the springs operate in a direction always perpendicular to the vehicle longitudinal axis.

Symmetrical halves.- As previously discussed, the assumption of symmetry in the shield-half geometry and spring force distribution was made to simplify the analysis. However, due to near symmetry, it was found that either of the actual shield-half physical parameters such as inertial and geometrical characteristics (see fig. 4) could be input to the numerical solution for any given q, a_1 combination, only small differences resulting in the shield motion. By calculating shield-half inertias for a symmetrical configuration with the same

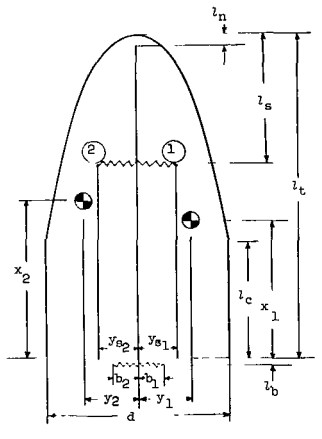

Parameter	Value of parameter for - Fire	Long Nimbus
x_1, in. (m)	45.20 (1.148)	93.33 (2.371)
x_2, in. (m)	50.10 (1.273)	96.24 (2.444)
y_1, in. (m)	14.60 (0.371)	17.86 (0.454)
y_2, in. (m)	13.90 (0.353)	17.68 (0.449)
I_{cg} ①, lbf-sec^2-in. (N-sec^2-m)	360.00 (40.670)	2964.00 (334.870)
I_{cg} ②, lbf-sec^2-in. (N-sec^2-m)	504.00 (56.940)	3324.00 (375.550)
Weight ①, lbf (N)	156.00 (693.920)	304.77 (1355.680)
Weight ②, lbf (N)	147.00 (653.890)	286.09 (1272.590)
l_c, in. (m)	24.50 (0.622)	131.50 (3.340)
l_t, in. (m)	117.00 (2.972)	224.00 (5.690)
l_n, in. (m)	10.03 (0.255)	10.03 (0.255)
l_s, in. (m)	76.00 (1.930)	76.00 (1.930)
l_b, in. (m)	0.68 (0.017)	0.68 (0.017)
y_{s_1}, in. (m)	12.25 (0.311)	12.25 (0.311)
y_{s_2}, in. (m)	11.88 (0.302)	11.88 (0.302)
b_1, in. (m)	1.03 (0.026)	1.03 (0.026)
b_2, in. (m)	1.00 (0.025)	1.00 (0.025)
d, in. (m)	62.43 (1.586)	62.43 (1.586)

Figure 4.- Nominal shield physical data.

mass per unit length characteristics as the short Nimbus or Fire shield, deployment trajectories were obtained for several q, a_l combinations. After comparing the motion of the near symmetrical halves with the motion of an assumed symmetrical half, the agreement indicated that use of the input data for shield 1, the shield without the nose cap (fig. 4), was acceptable for rigorous motion analysis. A parallel investigation was also conducted for the long Nimbus shield without nose cap.

Comparison with other work.- In lieu of experimental results to corroborate the analysis, and in order to verify further the use of actual shield data in the analysis, results for a 0.1g vehicular acceleration case without aerodynamic loading for one Fire shield half were compared with the results of an independent analysis of reference 4 which uses a simultaneous solution to solve for the shield-separation dynamics. This comparison yielded the agreement indicated in figure 5.

Aerodynamic Effects

The prime purpose of this paper in including aerodynamic influence is to ascertain whether this parameter is important in the upper atmosphere and to determine whether there is sufficient justification for requiring more appropriate aerodynamic data for specific applications. None of the available published reports on shield deployment (such as refs. 4 and 5) treat the influence of aerodynamic forces. Although heat shields are generally deployed at very high altitudes, it will be shown that significant influences on deployment trajectories can be experienced even with very low dynamic pressures. In the application of this analysis where consideration is given to the importance of aerodynamic loading, it should be observed that induced aerodynamic loading resulting from deployment velocities ($\dot{\theta}$, $\dot{y}$, $\dot{x}$) have not been considered; consequently, results for cases in which aerodynamic loading is present are valid only when the shroud velocities are small compared with the velocity of the moving coordinate system.

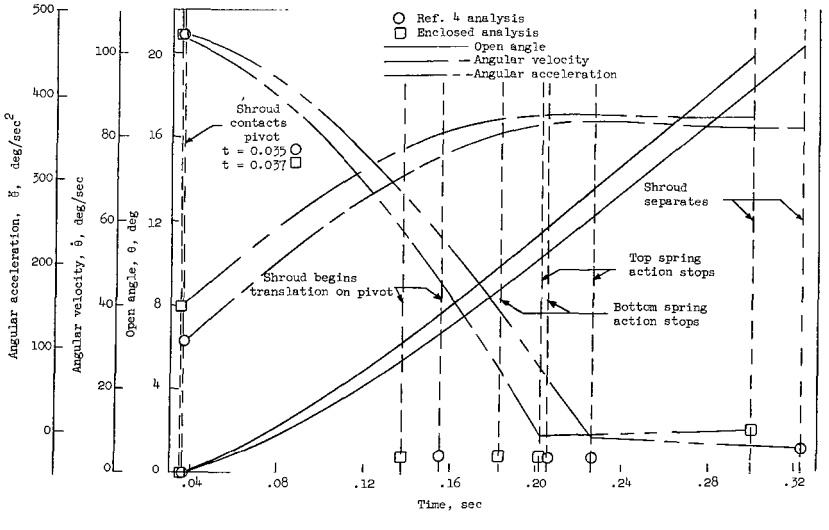

Figure 5.- Comparison of analytical results for Fire or short Nimbus shield without nose cap for a case of 0.1g vehicular acceleration and zero dynamic pressure.

The aerodynamic characteristics of the complex time-varying geometry presented by the opening clamshell design are not amenable to analytical solution. These characteristics can only

be adequately discerned from elaborate tunnel simulations or approximated from a wide source of similar geometries. The aerodynamic data used herein and presented in figures 6 and 7 are considered to be good engineering estimates and

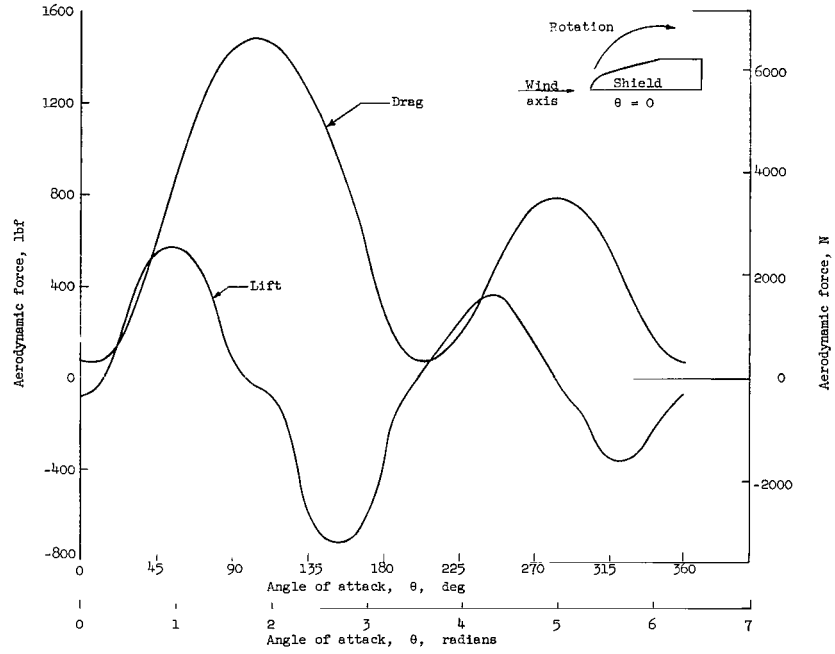

Figure 6.- Estimated aerodynamic characteristics. Fire shield.

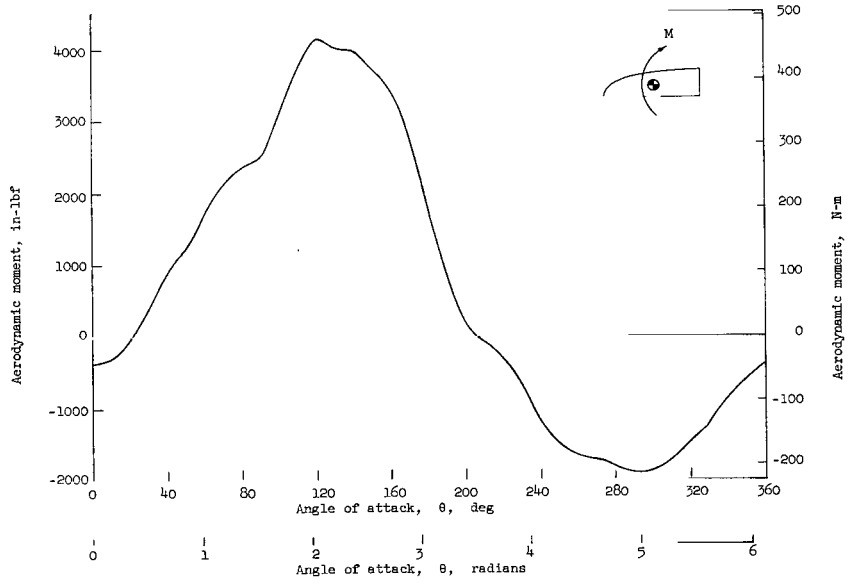

Figure 7.- Estimated aerodynamic moment. Fire shield.

were obtained by extrapolation of wind-tunnel data (refs. 9 and 10) from models similar to the short Nimbus heat-shield halves used with Project Fire. These data do not include interference effects which might occur between shield halves during the early phases of opening and between a shield half and parent vehicle prior to movement away from the immediate vehicle region. Also, in establishing the aerodynamic characteristics, the aerodynamic center and the planform centroid were assumed to be coincident for the shield half (ref. 10). In order to ensure the adequacy of the assumed aerodynamics used in the analysis, individual variations in aerodynamic lift and drag, respectively, were examined for a representative q,a_ζ case. The results, as presented in the following table, indicate that the lift parameter variation of ±20 percent caused a corresponding clearance change of 6.9 percent and -7.7 percent. The drag parameter variation of ±20 percent caused a clearance change of only -1.98 percent and 1.51 percent. Therefore, although changes in the lift parameter have a greater effect on clearance, neither parameter variation affected the clearance distance appreciably.

Aerodynamic variation, percent of nominal*		Clearance		Percent clearance change from nominal
L	D	Inches	Meters	
Nominal	Nominal	138.046	3.506	-----
20	Nominal	147.564	3.748	6.9
-20	Nominal	127.412	3.236	-7.7
Nominal	20	135.310	3.437	-1.98
Nominal	-20	140.134	3.559	1.51

*Nominal case: $a_\zeta = 0.1g$; $q = 1.65$ lbf/ft^2 (79,002 N/m^2)

q,a_ζ Combinations

Separation bounds.- In the following investigation, the aerodynamic q effect on shield deployment is considered with the a_ζ loading since the two conditions occur in combination for actual launch vehicle trajectories. Figure 8 indicates the limiting q,a_ζ combinations under which separation can theoretically be effected for the Fire and long Nimbus shields by using the nominal spring actuator characteristics. The boundary line outside of which separation theoretically cannot occur is established by whether $\dot{\theta}$ vanishes during phase 2 or phase 3. The spring locations are shown in figure 4, and the characteristics are given in the following table:

Spring	k		Remarks
	lbf/in.	N/m	
Forward spring actuator	15.644	2739.67	Same values for Fire and long Nimbus
Aft kickoff spring	102.564	17961.62	

Results (fig. 8) show that at zero q, the long shield can be separated at a greater vehicle a_l level than the Fire shield. Two primary reasons for this anomaly are the facts that (1) the long shroud center of gravity can be driven over "top dead center" ($\theta + \theta_{co} = 90^\circ$) by rotating the shield through a smaller angle than is possible for the shorter shroud, and (2) the inertial characteristics of the longer shield in rotation are more favorable than those for the shorter shield in sustaining motion once motion is initiated. (See fig. 4.) The larger aerodynamic influence on the long Nimbus shield accounts for the increased sensitivity to dynamic pressure indicated by the greater negative slope of the curve for the long Nimbus shield in figure 8. In establishing separation bounds, notice also that in the initial phases of motion, the aerodynamic lift as well as drag oppose separation as shown by the negative lift force for $\theta < 12.5^\circ$ ($\theta < 0.218$ radian) in figure 6.

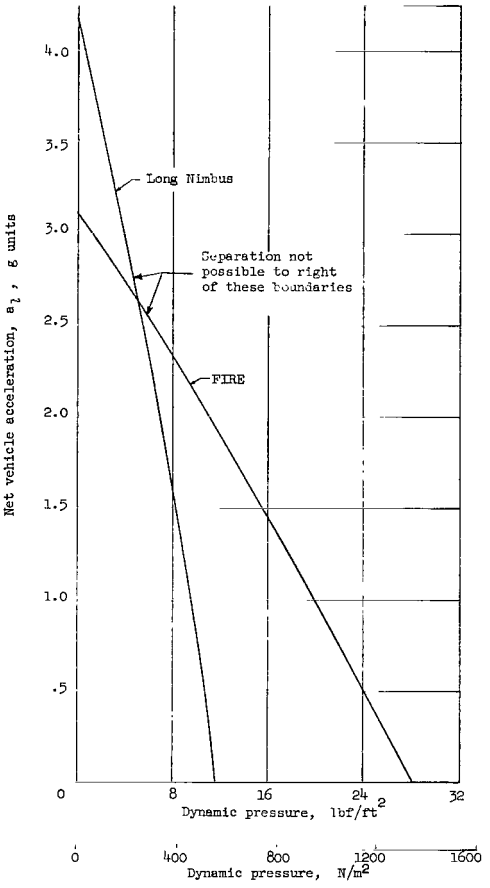

Figure 8.- Locus of limiting conditions for separation. Fire and long Nimbus shields.

Atlas trajectory parameters.- Since the Nimbus-type shield is commonly used on the Atlas launch vehicle, it is useful to present the possible flight times in a nominal Atlas trajectory during which the respective short and long shields can be deployed. These flight times can be ascertained by relating the limiting conditions from figure 8 to the actual trajectory conditions, the results being presented in figure 9. Separation is theoretically possible for a short time interval t_1 immediately after launch. With the exception of possible applications to low-altitude abort systems, however, normal mission requirements will generally dictate shield separation subsequent to maximum q. Although results indicate separation is feasible in the interval t_2 following BECO (Booster Engine Cutoff), it is obvious that the least complicated separation and greatest post separation clearance will be obtained in the nonthrusting region t_3 subsequent to SECO (Sustainer Engine Cutoff).

Post Separation Clearances

The clearance criterion.- The fact that either shield can be theoretically deployed at any q, a_l combination within its respective envelope describing the limiting cases (fig. 8) does not necessarily imply that all these combinations are acceptable. For the possible separation conditions, another criterion to be satisfied is that the post separation trajectory of this type of shield satisfy a predetermined minimum safe clearance requirement.

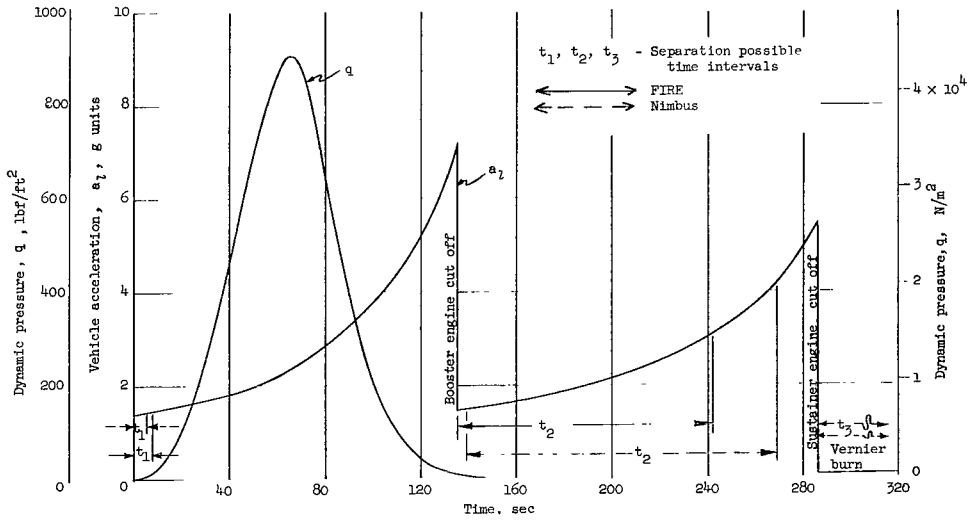

Figure 9.- Possible separation times during nominal Atlas trajectory. Long Nimbus and Fire shields.

Shield trajectory.- Shield clearance trajectories are presented in figures 10 and 11 for several assumed flight loading cases. For clarity, the shield tumbling motion has been shown for one case in each figure. The rotational velocity of the deployed shield yields a series of minima in the curve defining the clearance. These minima are defined as first minimum, second minimum, etc., as they progress downstream in relation to the parent vehicle. These typical points are indicated by the circular symbols on the $q = 16.5$ lbf/ft^2 (790.023 N/m^2) curve of figure 10. The a_l values shown thereon indicate the vehicular inertial accelerations.

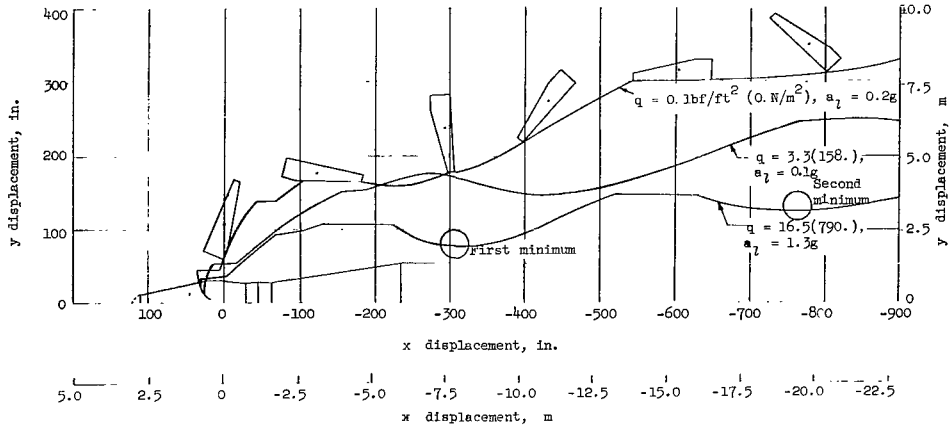

Figure 10.- Typical near point clearance trajectories. Fire shield with Atlas vehicle.

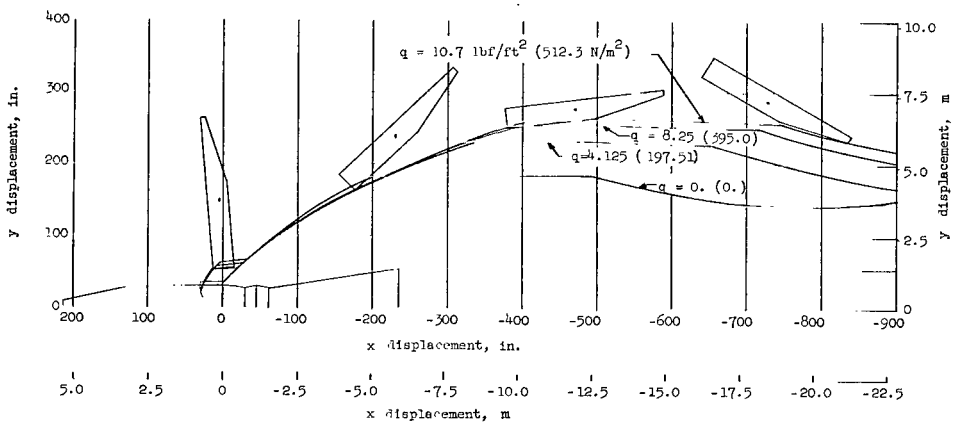

Figure 11.- Typical near point clearance trajectories for 0.4g acceleration with varying aerodynamic loads. Long Nimbus shield with Atlas vehicle.

Comparison of clearance data for q,a_l conditions.- The clearances as described graphically in figures 10 and 11 are presented in figures 12 and 13, respectively, for a number of separation-possible q,a_l conditions. The reason for the horizontally asymptotic behavior of the low q curves is that the separation angle for both long and short shields under low q, low a_l conditions causes shield post separation trajectories which are nearly perpendicular to the vehicle flight path. It is interesting to note from figure 12 that for all nonzero q cases shown, a constant first minimum clearance is indicated at the point of 0.45g vehicular acceleration. A similar condition exists for the long Nimbus shield at a vehicle acceleration of 0.1g. Since the minimum clearance specified by the booster contractor for Project Fire was 120 inches (3.048 m), it is apparent from figure 12 that this clearance can only be obtained for very low q,a_l combinations. From figure 13, it is seen that when the longer shield is used, a greater latitude in parameter selection will provide the prescribed 120-inch (3.048 m) clearance.

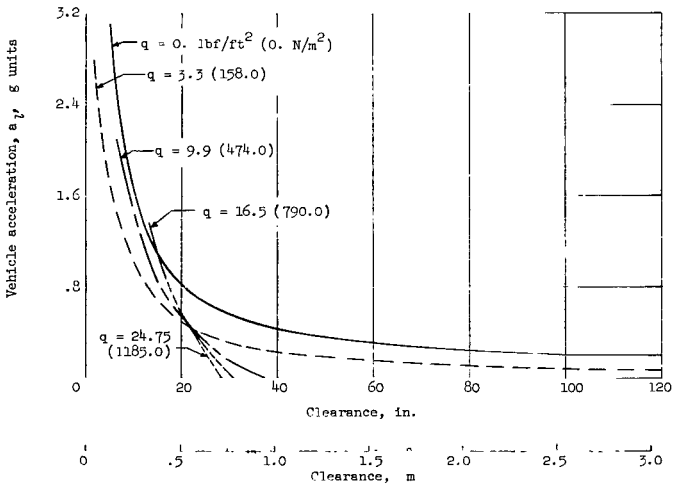

Figure 12.- First minimum clearance. Fire shield to Atlas vehicle.

Constant-clearance loci.- Families of curves for common first minimum clearances have been extracted from data such as those given in figures 12 and 13 and are presented in figures 14 and 15 for the short and long shields, respectively. The dotted curve of figure 14 corresponds to the point of common intersection noted for the curve families of figure 12. The corresponding condition for

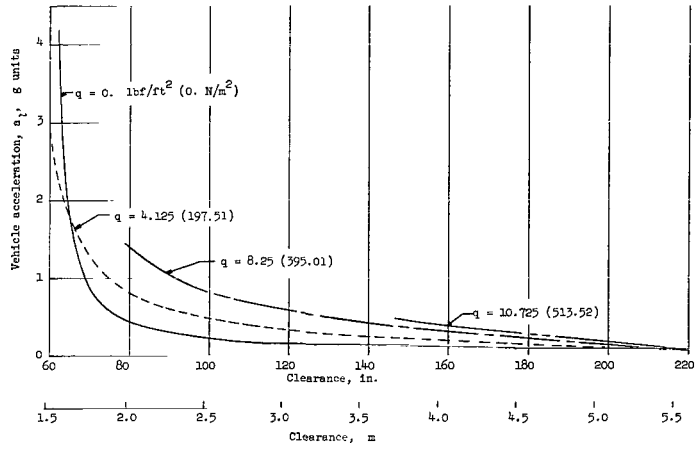

Figure 13.- First minimum clearance. Long Nimbus shield to Atlas vehicle.

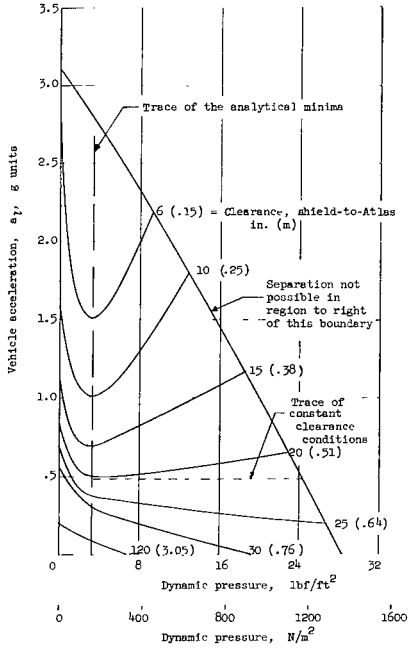

Figure 14.- Loci of common near point first minimum clearance for separation-possible conditions. Fire shield.

the longer shield is given by the 220-inch (5.588 m) clearance curve of figure 15. Notice, however, that figure 14 indicates that as q increases from zero to approximately 3.3 lbf/ft^2 (158,00 N/m^2) for a given g load, post separation clearance is significantly decreased. For any a_l level greater than about 0.45g, a q-increase above 3.3 lbf/ft^2 (158.00 N/m^2) becomes a favorable factor for increased clearance. Also, for $a_l < 0.45g$, first minimum clearance tends to decrease with increase in dynamic pressure. To obtain maximum clearance, the results indicate that separation for the short shield should be effected as near as possible to the zero q, zero a_l condition. It should be noted that the 120-inch clearance, as required for the Project Fire mission, can only be obtained with the highly restrictive q,a_l combinations confined in the limited lower left-hand region of figure 14. Although the clearance family of curves for the long Nimbus shield is similar in shape to the family of curves for the short shield, it is seen from figures 14 and 15 that for the same q,a_l condition, the clearance values are considerably greater for the longer shield. Figure 15 also indicates that a 120-inch (3.048 m) clearance requirement can be satisfied with a wider variation of q,a_l combinations for the longer shield, ranging up to 10.2 lbf/ft^2 (488.4 N/m^2) and 0.68g. The analytical minimum of the fixed clearance loci

apparent in figures 14 and 15 represents the least desirable q,a_z combination under which separation can be effected with respect to clearance. For the Fire shield, this point occurs consistently for a dynamic pressure between 3 and 4 lbf/ft^2 (143.6 and 191.5 N/m^2). For the long Nimbus shield, the trace of analytical minima varies from zero to about 2 lbf/ft^2 (95.8 N/m^2). It is important here to note that in the region to the right of the bounding curves for figures 14 and 15, the shield would fail to eject. However, a discontinuous relationship exists here in that just to the left of the bounding curves, separation will occur and will yield the clearances indicated. In actual flights, of course, sufficient margins on both q and a_z should be considered to allow for design parameter uncertainties. In figure 15, to the right of the trace of the minima, an increase in q causes a significant increase in clearance. It appears that aerodynamic loading in this q,a_z region is very favorable to post separation clearance.

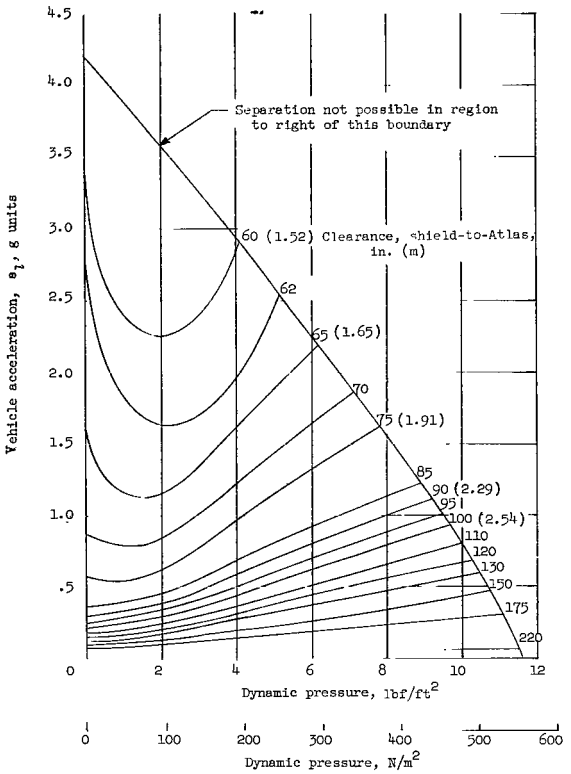

Figure 15.- Loci of common near point first minimum clearance for separation-possible condition. Long Nimbus shield. Some representative metric values of clearance are given by quantities in parenthesis.

Spring Energy Effects

The Nimbus shield configuration contains spring systems which are normally considered to be fixed in size and position in their respective components. For example, the forward springs, or thrusters, are located at the same longitudinal position relative to the shield nose regardless of shield length. Similarly, the aft kickoff springs are always located at the shield separation ring (fig. 4). Both forward and aft spring mechanisms are designed so that, for symmetrical halves, the spring forces always act in a direction perpendicular to the vehicle longitudinal axis.

An investigation to determine the effect of variations in spring constants on shield deployment yielded the q,a_z results indicated in figures 16 and 17 for the short and long shields, respectively, with the 100 percent or nominal spring curves replotted from figure 8. The curves describe the limiting conditions under which separation can be effected for the spring variations considered. It should again be noted that not all the possible separation conditions to the left of a bounding curve imply acceptable separation conditions in view of minimum clearance requirements.

Upper variation of the spring constants was kept within reasonable limits, as dictated by the mechanical configuration of the existing Nimbus shield. For the spring variations considered, the same percent change was applied to forward and aft springs. It should be noted, as is evident from figures 16 and 17, that appreciable increases in the magnitudes of separation-possible q,a_z combinations are obtained through increasing the nominal spring characteristics. Results of the spring-variation effect on minimum clearance of the Fire shield to the Atlas booster vehicle for a representative 8.25 lbf/ft^2 (395.01 N/m^2), 0.5g condition are plotted in figure 18. A similar curve is presented for the long Nimbus shield in figure 19 at the 8.25 lbf/ft^2 (395.01 N/m^2), 0.5g condition.

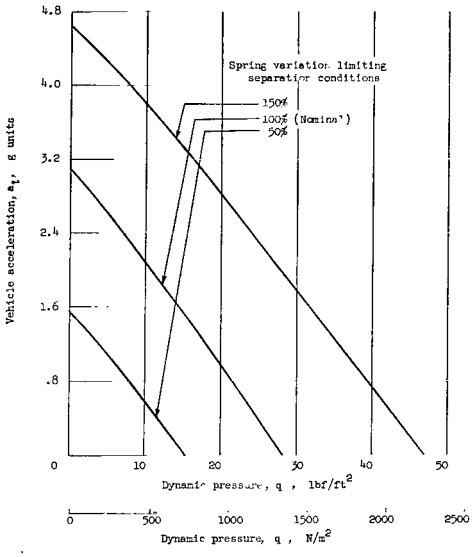

Figure 16.- Spring variation effect on limiting separation condition. Fire shield. Separation not possible in region to right of boundary for a given spring variation.

Even though appreciable changes in separation bounds were noted in figures 16 and 17 with changes in spring rates, it is apparent from the comparative curves of figures 18 and 19 that surprisingly little change in post separation trajectories would be obtained.

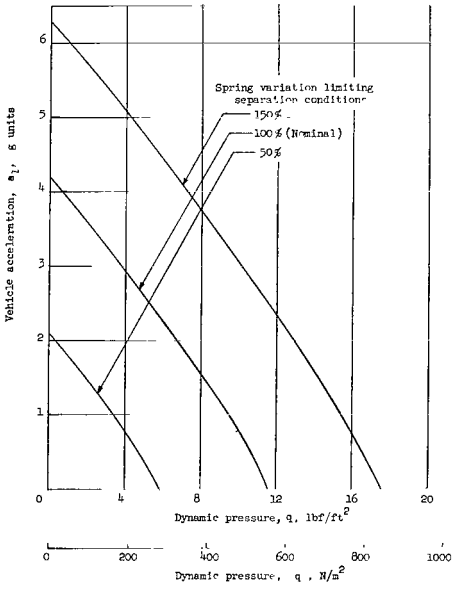

Figure 17.- Spring variation effect on limiting separation conditions. Long Nimbus shield. Separation not possible in region to right of boundary for a given spring variation.

Shield Length Effects

In the foregoing discussion, no direct comparisons of shield length effect on deployment have been presented. Since the Nimbus shield configuration is employed in many applications and proposals with length variation of the aft cylindrical portion as the only significant geometry change, two representative lengths have been selected and used throughout this investigation. The Fire shield is essentially a shortened version of the shield used on the Nimbus vehicle. The Nimbus vehicle shield is referred to as the long Nimbus shield. Some interesting results are obtained in comparing deployment for the two lengths with otherwise like structural and q,a_z conditions. Figure 20

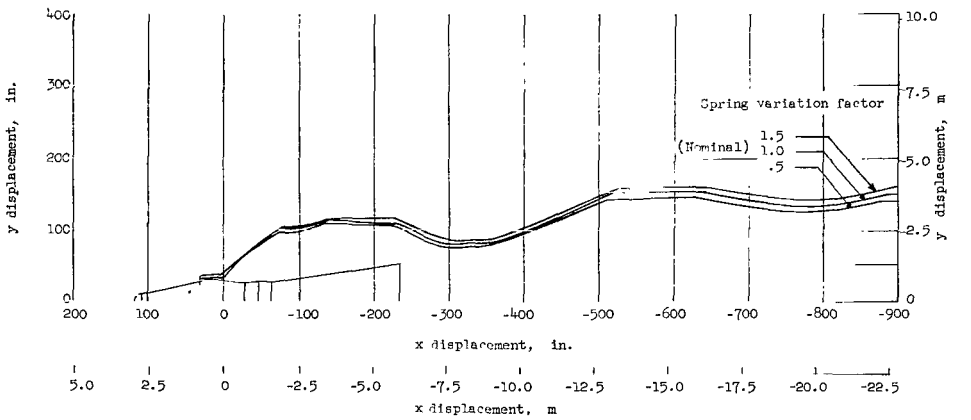

Figure 18.- Effect of spring variation on Fire shield near point trajectory for given q,a_{ζ} loading condition.

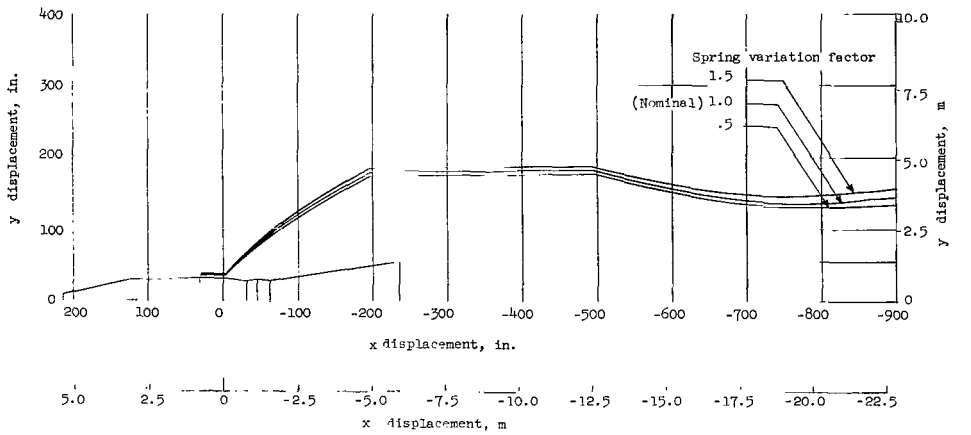

Figure 19.- Effect of spring variation on long Nimbus shield near point trajectory for a given q,a_{ζ} loading condition.

illustrates the wide difference in pitch rate between long and short shields for a representative q,a_{ζ} loading condition. Moreover, the advantages of the slow pitch rate are apparent in that the first minimum clearance is delayed until the longitudinal displacement is well beyond the parent vehicle. The unfavorable phasing of the pitch attitude of the short shield materially affects its minimum clearance (as is seen in fig. 20) at the downstream displacement of approximately 300 inches (7.62 m). For the inputs used in this phase of the analysis, the comparison of figure 20 shows that the long-shield deployment provides greater clearance than the short shield even though the two internal ejection systems have identical potential energy. The favorable deployment characteristics of the long shield are attributed principally to the increased aerodynamic normal force that aids separation and to the favorable angular attitude of the shield as it traverses the length of the launch vehicle. The helpful influence of the assumed aerodynamics was verified for the long Nimbus shield by comparing two cases with the same acceleration loading but with different dynamic pressure as shown in figure 21.

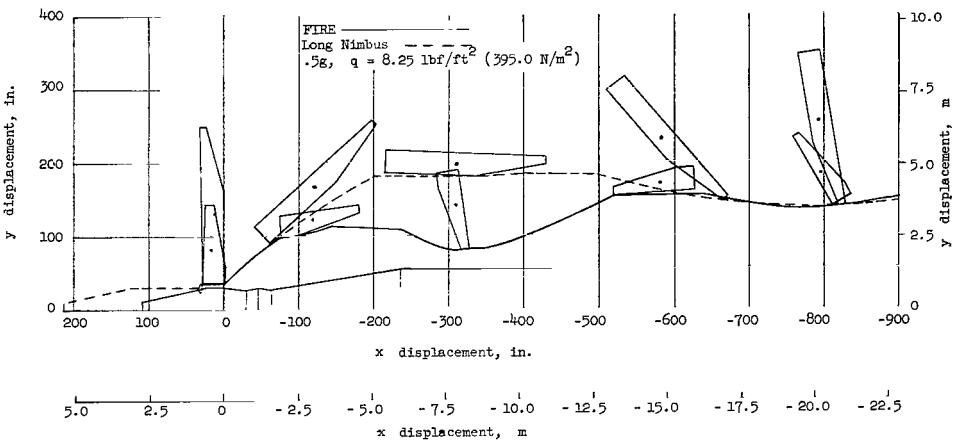

Figure 20.- Comparison of shield-length effect on post separation near point trajectory.

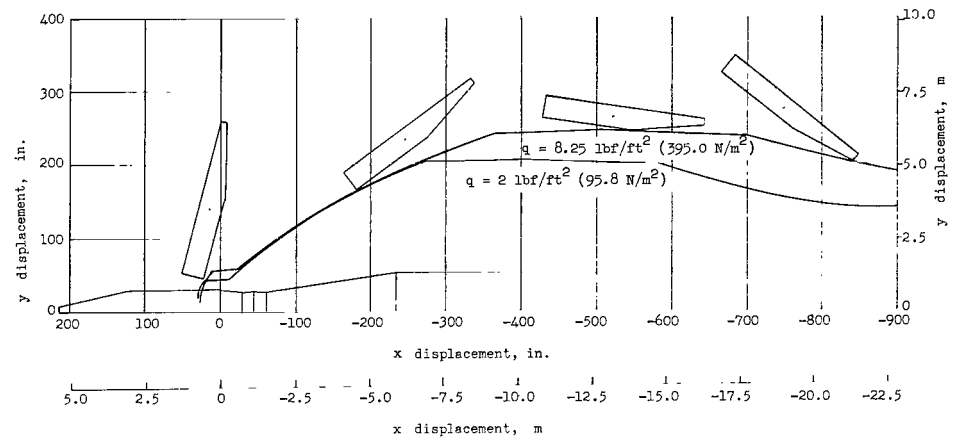

Figure 21.- Comparison of aerodynamic effect on post separation trajectory for 0.5g acceleration. Long Nimbus shield.

CONCLUDING REMARKS

An analytical investigation and parameter study have been made on a spring-actuated clamshell heat shield of the Nimbus type and the concluding remarks pertinent to the study are as follows:

1. Results indicate that deployment of the Nimbus configuration heat shield, in the lengths studied, is feasible under significant aerodynamic-pressure—vehicular-acceleration (q, a_l) combinations.

2. Aerodynamic lift and drag loading can be of definite advantage in the low vehicle acceleration region for effecting a greater clearance in the post separation trajectory.

3. The aerodynamic effect is more pronounced for the longer shield because of the increased planform area or lift.

4. The long Nimbus shield, although more limited in the separation-possible q,a_ζ loading envelope, will attain a more desirable clearance profile than the shorter Fire shield for a given q,a_ζ condition.

5. To obtain maximum clearance when used on the Atlas launch vehicle in a nominal trajectory, both short and long Nimbus shields should be deployed after sustainer engine cutoff.

6. Appreciable variation of the actuating spring rate affects the magnitude of q,a_ζ separation-possible conditions proportionally, but has negligible effect on the post separation trajectory.

7. The primary effect of shield length on deployment is in the shield rotational rate reduction at separation due to the increased rotational inertia associated with lengthening.

The approximate aerodynamics used in this study appreciably influence shield separation conditions and trajectories when deploying in the detectable dynamic-pressure region. The significance of the aerodynamics indicates the importance of obtaining accurate wind-tunnel data on the aerodynamic characteristics of a clamshell heat-shield configuration for various stages of opening.

Langley Research Center,
National Aeronautics and Space Administration,
Langley Station, Hampton, Va., November 2, 1965.

APPENDIX A

NUMERICAL METHOD FOR SOLUTION OF THE PHASE 2 ROTATION EQUATION OF MOTION

The step-solution recurrence relations valid for solution of the initial value propagation problem, when linear acceleration in the interval is assumed and the time interval is considered as the independent variable, are as follows:

$$\dot{\theta}_{n+1}^{(k)} = \left[\dddot{\theta}_n^{(k)}\Delta t\right]\frac{\Delta t}{2} + \ddot{\theta}_n\Delta t + \dot{\theta}_n \tag{A1}$$

$$\theta_{n+1}^{(k)} = \left[\dddot{\theta}_n^{(k)}\Delta t\right]\frac{\Delta t^2}{6} + \ddot{\theta}_n\frac{\Delta t^2}{2} + \dot{\theta}_n\Delta t + \theta_n \tag{A2}$$

where

$$\dddot{\theta}_n^{(k)}\Delta t = \ddot{\theta}_{n+1}^{(k)} - \ddot{\theta}_n \tag{A3}$$

and k represents the kth iteration within a time step. Substitution of the expression for the third derivative into equations (A1) and (A2), and simplification yields

$$\dot{\theta}_{n+1}^{(k)} = \left[\ddot{\theta}_{n+1}^{(k)} + \ddot{\theta}_n\right]\frac{\Delta t}{2} + \dot{\theta}_n \tag{A4}$$

$$\theta_{n+1}^{(k)} = \left[\ddot{\theta}_{n+1}^{(k)} + 2\ddot{\theta}_n\right]\frac{\Delta t^2}{6} + \dot{\theta}_n\Delta t + \theta_n \tag{A5}$$

and from equation (24)

$$\ddot{\theta}_{n+1}^{(k)} = \frac{1}{I_O}\Bigg[\Bigg(k_a\Big\{A - r\Big[\cos\theta_{ro} - \cos\left(\theta_{n+1} + \theta_{ro}\right)\Big] - y_e\Big\}r\sin\left(\theta_{n+1} + \theta_{ro}\right)$$

$$+ k_b\Big\{B - p\Big[\cos\theta_{po} - \cos\left(\theta_{n+1} + \theta_{po}\right)\Big] - y_e\Big\}p\sin\left(\theta_{n+1} + \theta_{po}\right)$$

$$- \left[D_{n+1}^{(k)} + a_l m\right]c\cos\theta_{co} + L_{n+1}^{(k)}c\sin\left(\theta_{n+1} + \theta_{co}\right) + M_{n+1}^{(k)}\Bigg)\Bigg] \tag{A6}$$

APPENDIX A

The method of solution is as follows: By using the initial conditions of θ_o, $\dot{\theta}_o$, $\ddot{\theta}_o$, and an arbitrary value as an initial choice for $\ddot{\theta}_{n+1}^{(k)}$, equation (A5) can be solved. Equation (A6) is then solved by proper selection of L, M, and D as determined by $\theta_{n+1}^{(k)}$. The next step is to obtain an improved value of $\ddot{\theta}_{n+1}^{(k)}$ by equation (A6). The process is repeated until convergence in $\ddot{\theta}_{n+1}$ is obtained. By using this value, equation (A4) is then solved. Also, at the end of each time increment, the following relations to determine whether the spring extensions are maximum must be evaluated:

$$\left| A - r\left[\cos \theta_{ro} - \cos\left(\theta_{n+1} + \theta_{ro}\right)\right] - y_e \right| \leqq \epsilon_1 \tag{A7}$$

$$\left| B - p\left[\cos \theta_{po} - \cos\left(\theta_{n+1} + \theta_{po}\right)\right] - y_e \right| \leqq \epsilon_2 \tag{A8}$$

where ϵ_1 and ϵ_2 are prescribed positive limits ≈ 0. Since the arbitrary value of Δt selected for the problem may not permit these relations to be satisfied at given time increments to within the predetermined error bounds ϵ, a method of subsequent halving of Δt is used as follows: If, in proceeding with the solution, a time increment is taken in which a change of sign occurs in the sum of the left-hand terms of relations (A7) or (A8), the solution has proceeded beyond the limit, and it is necessary to return to the time step prior to the occurrence of sign change, halve Δt, and proceed as before, with the new Δt. The sequence is continued until either of equations (A7) or (A8) is satisfied, at which time the term involving that relation $(k_a$ or $k_b)$ vanishes from equation (A6). When both equations (A7) and (A8) have been satisfied in this manner, the step solution is then continued with the original Δt until translation on the pivot begins.

APPENDIX B

NUMERICAL METHOD FOR SOLUTION OF THE PHASE 3 EQUATION OF MOTION DESCRIBING TRANSLATION ON PIVOT

The noniterative recurrence relations for the translational acceleration, displacement, and velocity on the pivot, with the assumption of linear acceleration, are as follows:

$$\ddot{e}_{n+1} = \left[\left(\frac{k_a}{m}\left\{A - y_e - r\left[\cos\theta_{ro} - \cos\left(\theta_{n+1} + \theta_{ro}\right)\right]\right\} + \frac{k_b}{m}\left\{B - y_e - p\left[\cos\theta_{po} - \cos\left(\theta_{n+1} + \theta_{po}\right)\right]\right\} - \left[\ddot{\theta}_{n+1}\left(x^*\cos\theta_{n+1} + h\sin\theta_{n+1}\right) + \dot{\theta}_{n+1}^2\left(h\cos\theta_{n+1} - x^*\sin\theta_{n+1}\right)\right] + \frac{L_{n+1}}{m}\right)\right](\sin\psi - \mu_s\cos\psi) - \left\{\left[\ddot{\theta}_{n+1}\left(h\cos\theta_{n+1} - x^*\sin\theta_{n+1}\right) - \dot{\theta}_{n+1}^2\left(x^*\cos\theta_{n+1} + h\sin\theta_{n+1}\right) + D_{n+1} + a_l m\right]\right\}(\cos\psi + \mu_s\sin\psi) \tag{B1}$$

$$\dot{e}_{n+1} = \left(\ddot{e}_{n+1} + \ddot{e}_n\right)\frac{\Delta t}{2} + \dot{e}_n \tag{B2}$$

$$e_{n+1} = \left(\ddot{e}_{n+1} + 2\ddot{e}_n\right)\frac{\Delta t^2}{6} + \dot{e}_n\Delta t + e_n \tag{B3}$$

Each time equation (A6) is solved for $\ddot{\theta}_{n+1}$ convergence, the resulting value is used to solve equations (A4) and (A5) as before. Substitution of these quantities and the resulting aerodynamic effects thus permit direct solution of equations (B1) to (B3) for each time interval. When the shroud has translated on the pivot a distance e_r, against which quantity equation (B3) is checked at the end of each time interval, shield deployment is effected. Notice that the interval halving scheme may again be required in order to obtain $e_{n+1} = e_r$ to within the prescribed error.

APPENDIX C

NUMERICAL METHOD FOR SOLUTION OF THE PHASE 4 FREE-FLIGHT EQUATIONS OF MOTION

By the same iterative method as employed in phase 2, convergence is now obtained on $\ddot{\theta}$ for each time step by the following equations:

$$\dot{\theta}_{n+1}^{(k)} = \left[\ddot{\theta}_{n+1}^{(k)} + \ddot{\theta}_n\right]\frac{\Delta t}{2} + \dot{\theta}_n \tag{C1}$$

$$\theta_{n+1}^{(k)} = \left[\ddot{\theta}_{n+1}^{(k)} + 2\ddot{\theta}_n\right]\frac{\Delta t^2}{6} + \dot{\theta}_n \Delta t + \theta_n \tag{C2}$$

$$\ddot{\theta}_{n+1}^{(k)} = \frac{M_{n+1}^{(k)}}{I_{cg}} \tag{C3}$$

from equation (47) where k again denotes the kth iteration within a time step. At convergence on $\ddot{\theta}_{n+1}$ for each Δt, selection of L and D at the corresponding angular displacement θ_{n+1} permits direct solution of the following noniterative recurrence relations:

$$\ddot{y}_{n+1} = \frac{L_{n+1}}{m} \tag{C4}$$

from equation (45)

$$\dot{y}_{n+1} = \left(\ddot{y}_{n+1} + \ddot{y}_n\right)\frac{\Delta t}{2} + \dot{y}_n \tag{C5}$$

and

$$y_{n+1} = \left(\ddot{y}_{n+1} + 2\ddot{y}_n\right)\frac{\Delta t^2}{6} + \dot{y}_n \Delta t + y_n \tag{C6}$$

Also

$$\ddot{x}_{n+1} = -\frac{1}{m}\left(D_{n+1} + a_l m\right) \tag{C7}$$

from equation (46),

$$\dot{x}_{n+1} = \left(\ddot{x}_{n+1} + \ddot{x}_n\right)\frac{\Delta t}{2} + \dot{x}_n \tag{C8}$$

and

$$x_{n+1} = \left(\ddot{x}_{n+1} + 2\ddot{x}_n\right)\frac{\Delta t^2}{6} + \dot{x}_n \Delta t + x_n \tag{C9}$$

The process is continued as long as required. The limit imposed could be some maximum value of time or displacement as required.

REFERENCES

1. Scallion, William I.; and Lewis, John H., Jr.: Flight Parameters and Vehicle Performance for Project FIRE Flight 1, Launched April 14, 1964. NASA TN D-2996, 1965.

2. Thomson, W. T.: Missile Separation Dynamics. TR-59-0000-00824, Space Technol. Labs., Inc., Oct. 1, 1959.

3. Solarski, A. H.; Turner, R.; and Doerr, F.: Dynamics of Separating Bodies. Vol. I - Theoretical Analysis. AFOSR-109, U.S. Air Force, Mar. 1961.

4. Christensen, K. L.: Separation Analysis Project Fire Shroud. Rept. No. SM-42639 (Contract No. CVC-341, NAS 1-1946), Douglas Aircraft Co., Inc., Apr. 1963.

5. Anon.: AVT Analysis Handbook Echo A-12 AVT Project. Rept. No. SM-38881 (Contract No. NASw-38), Douglas Aircraft Co., Inc., Aug. 1961.

6. McKee, John W.: Analog Investigation of Longitudinal Flight-Path Characteristics of an Airplane Nose Section Serving as an Escape Capsule. NASA TM X-679, 1962.

7. Janos, Joseph J.; and Unangst, John R.: Effect of Lift on Separation Distance and Loads for an Aborting Vehicle at Maximum Dynamic Pressure of a Lunar Mission. NASA TN D-1775, 1963.

8. Mechtly, E. A.: The International System of Units - Physical Constants and Conversion Factors. NASA SP-7012, 1964.

9. Armstrong, William O.: Hypersonic Aerodynamic Characteristics of Several Series of Lifting Bodies Applicable to Reentry Vehicle Design. NASA TM X-536, 1961.

10. Wiggins, Lyle E.; and Kaattari, George E.: Supersonic Aerodynamic Characteristics of Triangular Plan-Form Models at Angles of Attack to 90°. NASA TM X-568, 1961.

"The aeronautical and space activities of the United States shall be conducted so as to contribute . . . to the expansion of human knowledge of phenomena in the atmosphere and space. The Administration shall provide for the widest practicable and appropriate dissemination of information concerning its activities and the results thereof."

—NATIONAL AERONAUTICS AND SPACE ACT OF 1958

NASA SCIENTIFIC AND TECHNICAL PUBLICATIONS

TECHNICAL REPORTS: Scientific and technical information considered important, complete, and a lasting contribution to existing knowledge.

TECHNICAL NOTES: Information less broad in scope but nevertheless of importance as a contribution to existing knowledge.

TECHNICAL MEMORANDUMS: Information receiving limited distribution because of preliminary data, security classification, or other reasons.

CONTRACTOR REPORTS: Technical information generated in connection with a NASA contract or grant and released under NASA auspices.

TECHNICAL TRANSLATIONS: Information published in a foreign language considered to merit NASA distribution in English.

TECHNICAL REPRINTS: Information derived from NASA activities and initially published in the form of journal articles.

SPECIAL PUBLICATIONS: Information derived from or of value to NASA activities but not necessarily reporting the results of individual NASA-programmed scientific efforts. Publications include conference proceedings, monographs, data compilations, handbooks, sourcebooks, and special bibliographies.

Details on the availability of these publications may be obtained from:

SCIENTIFIC AND TECHNICAL INFORMATION DIVISION

NATIONAL AERONAUTICS AND SPACE ADMINISTRATION

Washington, D.C. 20546